PARTICLE MOTION OF COATED CORN SEED ACCUMULATION PROCESS BASED ON DISCRETE ELEMENT METHOD
/
基于离散元法的包衣玉米种子堆积过程颗粒运动研究

Shihao WANG [1)], Shouhao XIA [1)], Yongxin CHEN [1)], Chao LOU [1)], Dinglin REN [1)], Zhaodong LI*[1, 2)]
[1)] College of Engineering, Anhui Agricultural University, Hefei, Anhui, 230036, China
[2)] Engineering Laboratory of Intelligent Agricultural Machinery Equipment, Anhui, Hefei, 230036, China
Tel: +86 13675606219; E-mail addresses: Lizd@ahau.edu.cn
DOI: https://doi.org/10.35633/inmateh-72-34

Keywords: *model of particles; corn; angle of repose; liquidity; discrete element method*

ABSTRACT
The rolling friction coefficient was a fundamental parameter for particle modeling, but it was challenging to quantify for unevenly shaped corn seeds. If the rolling friction coefficients of corn with different guiding seeds and different shapes were not believed to be significantly different, direct simulation in EDEM would produce simulation distortion. This paper began by selecting three models with a relatively high proportion from five corn samples with various shapes (such as horse-tooth shape, spherical shape, oblate shape, and irregular shape, etc.) and modeling them according to the actual seeds. Due to the large disparity between seed models with different shapes, the study adopted the method of combining physical experiment and discrete element simulation, took the rolling friction coefficient as the independent variable and the angle of repose in the simulation test as the target value, and calibrated the rolling friction of various shapes of corn seed particles separately. Coated corn seeds' rolling friction coefficients were accurately predicted (0.0047 for horse tooth, 0.0058 for pyramid, and 0.049 for spherical shape). During the validation test, the calibrated simulation parameters were entered into EDEM for simulation, and the distribution of seeds on the seed platter was compared between the actual test and the simulation test. The results demonstrated that the difference in the sizes of key features was less than 5.60 percent, and the population boundary in the seed platter after calibration was closer to the actual situation, which improved the accuracy of the simulation.

摘要
滚动摩擦系数是进行颗粒模拟的基础参数，但对于形状不规则的玉米种子，滚动摩擦系数难以测量。如果不考虑模型形状的不同导种不同形状玉米之间的滚动摩擦系数有较大差异，直接在 EDEM 中进行仿真，会出现仿真失真的情况。针对此问题，本文首先从五种不同形状的玉米样品（如马齿形、球形、扁球形和不规则形状等）选出三种较为典型且占比较高的模型，根据实际种子进行建模。由于不同形状种子模型的差距较大，本文采用物理实验和离散元仿真结合的方法，以滚动摩擦系数为自变量，以仿真试验的休止角为目标值，将几种不同形状玉米种子颗粒的滚动摩擦进行了单独标定，详细预测包衣玉米种子的滚动摩擦系数(马齿形为 0.0047、棱锥形为 0.0058、类球形为 0.049）。同时研究了包衣玉米种子滚动摩擦系数和颗粒形状对休止角形成过程的影响，提取了种群势能和平均速度，结果表明滚动摩擦系数可以改变种群流动性，增加玉米种子休止角形成的时间；玉米形状不同对休止角形成过程的作用不同，流动性较差马齿状可以很好的增加种子堆的高度和休止角，流动性较好的类球形则会增大堆积范围。在验证试验中，将标定的仿真参数输入 EDEM 中进行仿真，对比实际试验与仿真试验排种器内种子的分布情况，结果表明：关键特征尺寸数值差异在 5.6%以内标定后的排种器内种群的边界与实际情况更接近，提高了仿真的可靠性，为气力式玉米排种器离散元研究提供了理论依据。

INTRODUCTION
Corn is an important grain, oil, and feed crop that plays a significant role in agricultural output (*Shi et al., 2014*). The quality of the seeds ensures a stable and abundant harvest. In order to ensure the quality of seeds, researchers need to do a lot of analysis of the seeding process.

Shihao Wang, U.G. Stud.; Shouhao Xia, M.S. Stud.; Yongxin Chen, Prof.;
Chao Lou, M.S. Stud.; Dinglin Ren, M.S. Stud.; Zhaodong Li, Assoc. Prof

The processes of seed filling, seed clearing, seed carrying, and seed casting of the corn seed in the seeding process through the seeder were all discrete particle movements (*Ding et al., 2019*). The contact movement process between seeds and seeds, as well as between seeds and the seed-metering device, was rather complicated in the preceding procedure. Using the discrete element method (DEM) to examine the migration law of the seed-metering device in the seed drainer during the seed drainage process (*Owen and Cleary, 2012*).

Establishing a more precise seed particle model is necessary for discrete element simulation (*Chen et al., 2018*). Using the polyhedron filling approach (*Wang et al., 2022),* they created six sunflower seed multi-sphere models with varying accuracy (25, 28, 31, 34, 37, and 40 subspheres), and the results indicate that the 31-sphere model is more consistent with the real test results. Using the multi-sphere technique, *Zhou et al., (2020),* created four seed particle models of differing precision. The multi-ball model employs artificial roughness to assess its filling precision. On the basis of the combined spherical technique, *Li et al., (2020*), created a discrete elementary particle model for buckwheat seeds. *Wang et al., (2018)* established the discrete fundamental model of corn seeds and *Xu et al., (2020)*, constructed the discrete elementary model of soybean seeds, while *Zhang et al., (2022)*, got the shape of rice seeds using 3D scanning and reverse fitting. They constructed different rice seed particle radius models (0.30, 0.21, 0.18, 0.16, and 0.15 mm). Based on the volume distribution of peanuts, *Wu et al., (2020)*, built a simulation model of peanut seeds. *Ma et al., (2020)*, constructed the discrete element model of alfalfa seed and calibrated the discrete element parameters based on the actual shape of alfalfa seed.

The correct calibration of particle model parameters has a direct impact on the accuracy of discrete element simulation results (*Zhou et al., 2020*). Among these, the rolling friction coefficient is an essential parameter in the discrete element modeling of coated corn seed particles, the foundation of DEM particle simulation, and the foundation for building and enhancing particle processing machines. The coefficient of rolling friction is an essential physical property of corn particles. In the process of motion, the relative rolling of two objects generates rolling friction. Due to the uneven form of corn particles, it is difficult to determine the value of this coefficient (*Wang et al., (2018)*. It has been discovered that particle form and interparticle friction have a significant influence on the uniaxial compression behavior of materials. When rolling friction is applied, simulations of single-nozzle fluidized beds can be greatly enhanced *Goniva et al., (2012)*. The rolling friction force can lower the velocity of particles leaving a flat-bottom bin and influence particle accumulation (*Balevičius et al., 2012*). According to previous research, the relationship between rolling friction and rolling speed of a soft ball on a hard plane is nonlinear (*Yung and Xu, 2003),* and the friction coefficient grows linearly with the increase in average contact pressure until the maximum limit of the constant friction coefficient. (*Xiao et al., 2007*)

According to the aforementioned research, the quality of seed particle modeling and the calibration of seed parameters are the primary factors influencing the accuracy of simulation findings when discrete element simulation of corn seed particles is performed. Few studies, however, have used the discrete element method to investigate the effect of the interplay between seed particle morphologies and rolling friction coefficients on the angle of repose. Angle of repose is a macroscopic quantity that characterizes the flow, friction, and other properties of granular materials; it is related to the physical properties of contact materials and the materials themselves (*Boac et al., 2010)*. In agricultural engineering, it is typically used to calibrate material parameters, such as seeds and soil (*Wang et al., 2017*). In this study, the characteristic sizes of three distinct corn seed shapes were measured, and a strategy for establishing reliable seed models based on the positive distribution of the characteristic sizes was provided. The method ensured the precision of model construction and the efficiency of simulation time. The effects of various corn seed shapes and rolling friction coefficients on population migration were then investigated. It provided a theoretical basis for the design of a corn precision seed-metering device and the discrete element research of the law of orderly transport of corn seed particles in the corn precision seed-metering device.

MATERIALS AND METHODS

Establish particle contact mechanics model

Zhengdan 958, a commonly planted variety, was chosen for this investigation, and the drying process evaluated its moisture content, which was 12.7%. The moisture concentration of corn seed particles was lower; therefore, particle adhesion could be disregarded. To simulate the accumulation process of corn seeds, the rolling friction model related to relative velocity, namely the Hertz-Mindlin (no slip) contact model in EDEM software, was chosen (*Peng et al., 2018*).

Density, Poisson ratio, shear modulus, recovery coefficient, static friction coefficient, and rolling friction coefficient are the parameters of the Hertz-Mindlin model. The discrete element method simulates the propagation process of moving particles, and the movement of particles will inevitably result in collisions and force generation between particles. According to the different contact modes, the discrete element can be subdivided into hard ball contact and soft ball contact, and the soft particle contact model permits overlap between the contact points of two particles. The contact force can be calculated based on the amount of normal phase overlap and tangential displacement between particles, and the normal phase and tangential forces are closely related to the friction between particles. Therefore, this study employs the soft particle contact model, as illustrated in Fig. 1.

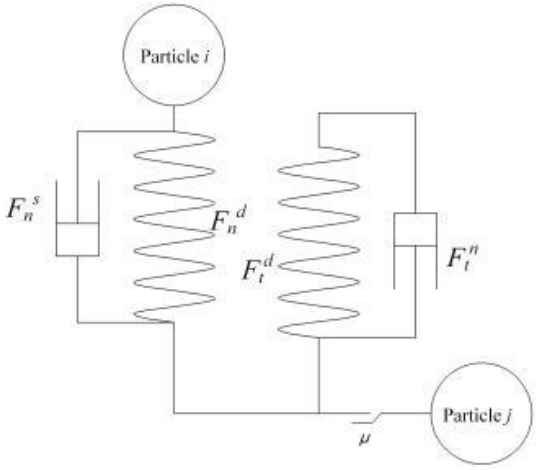

Fig. 1 - Particle-contact model

The definitions of normal contact force and tangential contact force are as follows:

$$F_n = F_n^s + F_n^d \quad (1)$$

$$F_t = F_t^s + F_t^d \quad (2)$$

where:

F_n is the normal contact force; F_t is the tangential contact force [N]; F_n^s is the elastic and viscous damping forces of vertical; F_n^d is the contact surface [N]; F_t^s is the static friction force; F_t^d is the dynamic friction force in the tangent direction of the contact surface [N].

$$F = \begin{cases} F_t \cdot if \cdot F_t < \mu \cdot F_n \\ \mu \cdot F_n^s \cdot if \cdot F_t < \mu \cdot F_n \end{cases} \quad (3)$$

where:

μ is the friction coefficient; F is the tangential total contact force.

After calculating F_n and F_t, the gravitational force is applied to these two forces to determine the resultant force. The resultant force F_{res} is calculated as follows:

$$F_{res} = F_n + F_t + mg \quad (4)$$

where:

m is the mass [g]; g is the gravitational acceleration of particles [m/s^2]; F_{res} is the resultant force on the particle [N].

Due to the fact that the tangential component of the contact force causes the torque effect M, the magnitude of the torque effect is calculated as the product of the tangential force F_t and the vertical distance between the contact point and the center of mass r (*Tanaka et al., 2000*). Consequently, the torque effect is determined as follows:

$$M = r \cdot F_t \quad (5)$$

$$r_{ij} = \frac{r_i \cdot r_j}{r_i + r_j} \quad (6)$$

where:

M is the torque generated by the tangential component of the contact force [N·m]; r_i, r_j are the equivalent diameters of particles i and j [mm].

In granular systems, rolling frictional drag consumes energy during relative rotation and provides packing support that stabilizes the granular system. Therefore, additional torques are applied to the contact surface.

$$M_r = -\mu_r \cdot F_n^s \cdot r \cdot \lambda_\theta \quad (7)$$

where:

M_r is the torque due to rolling friction [N·m]; μ_r is the coefficient of rolling friction; $\lambda_{\dot{\theta}}$ is the vector of angular velocity per unit time; $\dot{\theta}$ is the contact point angle [°].

The resultant torque M_{res} is as follows:

$$M_{res} = M + M_r \quad (8)$$

Newton's second law of motion is used to calculate the particle's acceleration in order to update its position. The particle's translational and rotational accelerations are as follows:

$$\ddot{a} = \frac{F_{res}}{m} \quad (9)$$

$$\ddot{\omega} = \frac{M_{res}}{I} \quad (10)$$

where:

$\ddot{a}$ is the particle translational acceleration [m/s²]; $\ddot{\omega}$ is the particle rotational acceleration [m/s²]; I is the moment of inertia of the particle [mm⁴].

After calculating the velocity, the new particle localization is determined by integrating the velocity over the time interval. The following are the definitions of normal and tangential contact forces and damping forces between two particles:

$$F_n^s = -K_n h^{\frac{3}{2}} \quad (11)$$

$$K_n = 2 \cdot E_{ij} \cdot \sqrt{r_{ij} \cdot a_{ijn}} \quad (12)$$

$$\frac{1}{E_{ij}} = \frac{(1-v_i^2)}{E_i} + \frac{(1-v_j^2)}{E_j} \quad (13)$$

where:

K_n is the normal stiffness; h is the normal component of relative displacement [mm]; E is the Young's modulus of the corresponding particle; v is the Poisson ratio of corresponding particles i and j.

Mindlin's definition of tangential contact forces:

$$F_s^t = -K_t \cdot h \quad (14)$$

$$K_t = 8 \cdot G_{ij} \sqrt{r_{ij} \cdot h} \quad (15)$$

$$\frac{1}{G_{ij}} = \frac{2-v_i}{G_i} + \frac{2-v_j}{G_j} \quad (16)$$

where:

K_t is the tangential stiffness defined by Mindlin; G is the shear modulus of particles i and j [g].

Then the normal damping and tangential damping forces are:

$$F_n^d = -2 \cdot \sqrt{\frac{5}{6}} \cdot \psi \cdot \sqrt{K_n \cdot m_{ij}} \cdot \dot{a}_{ijn} \quad (17)$$

$$F_t^d = -2 \cdot \sqrt{\frac{5}{6}} \cdot \psi \sqrt{K_n \cdot m_{ij}} \cdot \dot{a}_{ijt} \quad (18)$$

$$m_{ij} = \frac{m_i + m_j}{m_i \cdot m_j} \quad (19)$$

where:

ψ is the corresponds to the viscous damping coefficient in tangential and normal directions [N·m/s]; m is the mass of particles i and j [g].

When DEM is used to simulate the motion law of coated corn seeds, the rolling friction coefficient and restoration coefficient of the particle model are important parameters that affect the accuracy of different corn simulation models, and the rolling friction coefficient is an important parameter for studying the fluidity of different corn seed particle model shapes.

Analysis of the geometric shape of corn

Multi-contrast observation was used to classify Zheng-dan 958 corn seeds into horse-tooth shape, prism shape, spherical shape, spherical-cone and irregular shape. As depicted in Fig. 2. The upper and lower profiles of the horse tooth seed particles are trapezoidal, the overall thickness varies little, the width is significantly greater than its thickness, and the shape resembles horse teeth. The prism edge has four distinct edges and has the general shape of a cone; its thickness decreases gradually from base to apex, and its width is slightly greater than its thickness. The quasi-sphere can be represented as a sphere with a circle-like surface. The base of the cone is circular, while the upper portion is conical. Other than the aforementioned four, irregular shapes consist of all other shapes.

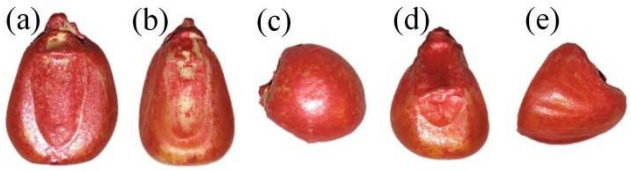

Fig. 2 - Geometrical shape classification of corn seeds of the same variety

(a) horse-tooth, (b)prism, (c) spherical, (d) spherical-cone, and (e) irregular shape.

One thousand seeds were selected at random and categorized according to their respective shapes. As illustrated in Fig. 3, the percentage of equine tooth-shape, prism shape, spherical shape, and irregular shape were 62.2%, 17.2%, 13.8%, 3.8%, and 3%, respectively, and the sum of equine tooth shape, prism shape, and spherical shape comprised approximately 93.2% of the total number of corn grains. The proportion of irregular and spherical conical seeds does not exceed 7%. Since the percentage of these two types of seeds is much lower than the percentage of the other three types of seeds, they are disregarded to simplify the modeling of corn seed particles in this paper.

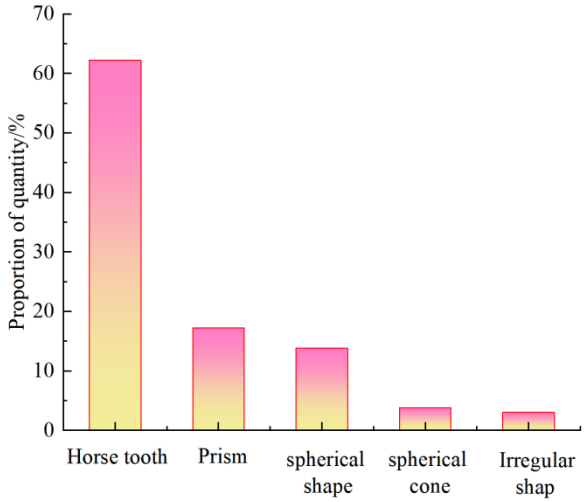

Fig. 3 - Percentage of each shape of corn seeds for Zheng-dan 958

Process for modeling corn seed particle and related analysis

Currently, numerous scientists establish the particle model of corn seeds using the sphere filling method (*Pasha et al., 2016*). In the model presented above, the arrangement and quantity of marbles are distinct. The calculation time increases as the number of marbles increases. However, this does not necessarily increase the accuracy of the model for corn seeds (*Urtė et al., 2016*). When the number of marbles reaches a certain threshold in practical applications, model accuracy and calculation time will converge to an acceptable level (*Wang et al., 2017*). There is currently no consensus on the arrangement and number of subfields, and the topic requires additional research. In addition, when establishing its particle model, some studies as for example *Wang et al., (2017)*, only select the triaxial size of corn seeds as the characteristic size. It is difficult to represent the physical characteristics of actual corn seeds.

This study examines coated corn as its research object. The various seed particle morphologies of coated corn were modeled. The size and distribution of corn particles are significant parameters because they affect the modeling basis. Through comparative observation, the corn seeds were divided into three representative shapes: horse-tooth shape, prism shape, and spherical shape. To more accurately model corn seed particles, the size and shape of the actual seed particles were determined.

In order to create a more precise corn model, the characteristic sizes of three distinct corn seed shapes were specified and measured. As illustrated in Fig. 4, the upper width W_1, lower width W_2, thickness T, and height H of horse tooth seeds were primarily measured. Compared to horse tooth seeds, the thickness of prism seeds was significantly altered; however, the overall thickness of horse tooth seeds remained the same, whereas prism seeds had a conical shape with a thicker base and a progressively thinner top. Therefore, the primary dimensions of prism seeds are the upper width W_1, the lower width W_2, the upper thickness T_1, the lower thickness T_2, and the height H, whereas the primary dimensions of spherical seeds are the vertical and horizontal diameters D_1 and D_2. The measurement histogram of the size distribution of three different types of corn seeds is shown in Fig. 5. Origin software is utilized during the fitting process. The fitting curve follows the normal distribution approximately, and the fitting equation is as follows:

$$f(x)=\frac{1}{\sqrt{2\pi}\sigma}e^{-\frac{(x-\mu)^2}{2\sigma^2}} \quad (20)$$

It is symbolized by the symbol N (μ,σ^2), where the horse tooth is W_2 *(9.42, 0.42)*, T *(6.34, 0.55)*, prism W_2 *(8.47, 0.47)*, T_2 *(6.36, 0.51)*, and spherical D_1 *(8.82, 0.51)*, D_2 *(9.08, 0.81)*.

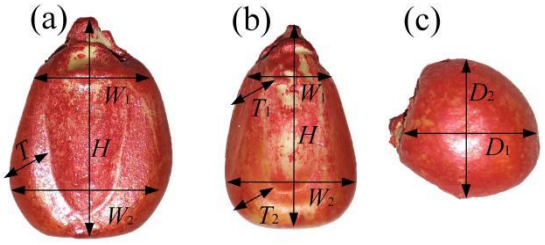

Fig.4 - Corn seed size and discrete element mode

(a) horse-tooth, (b) prism, and (c) spherical.

In the modeling process, pellets are used to determine the number of spheres required within the component to construct the simulated corn. Consequently, the issue is determining the size of each particle within the component used to simulate coated corn seed particles. Currently, some researchers are establishing the particle model of corn seeds via the sphere filling method, using 5, 10, 15, and 20 spheres, respectively, to establish their analysis models. In theory, as the number of spheres increases, the seed model will become closer to the actual seed. However, the study found that the calculation time increased as the number of spheres increased. This does not necessarily enhance the model accuracy of corn seeds, though. In practice, when a certain number of child spheres is reached, model accuracy and calculation time will converge to an acceptable level. In this study, a small number of spheres will be used to establish the seed simulation model so that it closely resembles the actual seed size.

Table 1

Modeling parameters of corn seed morphology

Seed shape	Mean of characteristic sizes						
	W_1	W_2	T_1	T_2	D_1	D_2	H
	[mm]	[mm]	[mm]	[mm]	[mm]	[mm]	[mm]
Horse-tooth	6.9	9.5	5.2	5.2			13.3
Prism	4.8	8.2	4.6	5.6			12.5
Spheroid					8.8	8.6	

The characteristic diameters of three types of seed model particles are displayed in Table 1. The multi-ball filling method of three-shaped corn seed particle models is produced according to the dimensions in Table 1, as depicted in Fig. 6 where (a) is a horse-tooth shape, (b) is a spherical shape, (c_1) is a prism shaped front view, and (c_2) is a prism shaped side view. The thickness of horse tooth seed is comparable to that of the diameter d_1 of the balls in the lower three rows of the horse-tooth shape, which was equal to the thickness of the horse tooth shape, which was 5.2 mm. The diameters of the balls in the upper two rows were d_2 = 4 mm and d_3 = 2 mm. Prism corn seeds were filled with small balls with a d_4 diameter of 4 mm and a d_5 diameter of 8.4 mm. As the thickness decreases gradually from bottom to top, the bottom two layers are filled with 3 mm d_6 balls. Because the thickness and width of the prism base differ, so does the distance between the corresponding balls. The upper width and depth of the prism corn seeds are comparable, so the upper layer is filled with d_8-diameter balls. In the middle, a d_7 = 4.6 mm ball is used for transition, while d_9 = 4.5 mm and d_{10} = 2.3 mm balls are used in the upper portion.

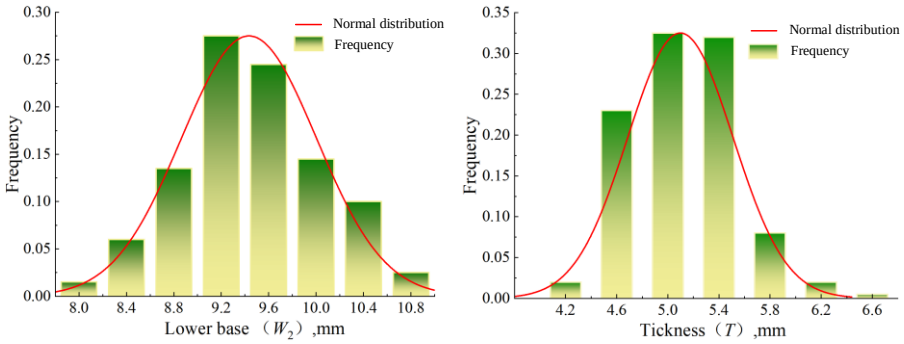

(a) horse-tooth shape

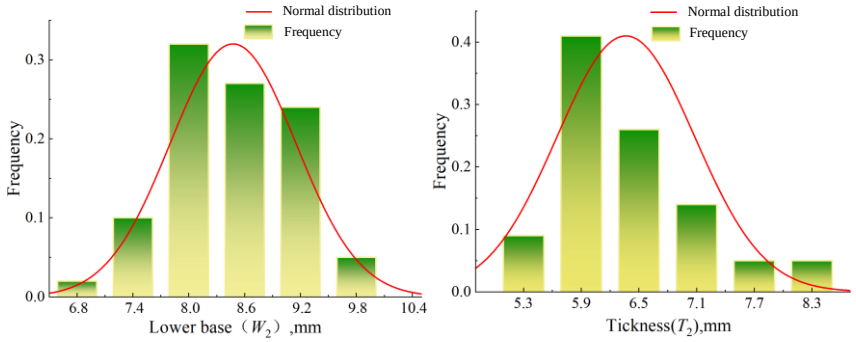

(b) prism shape

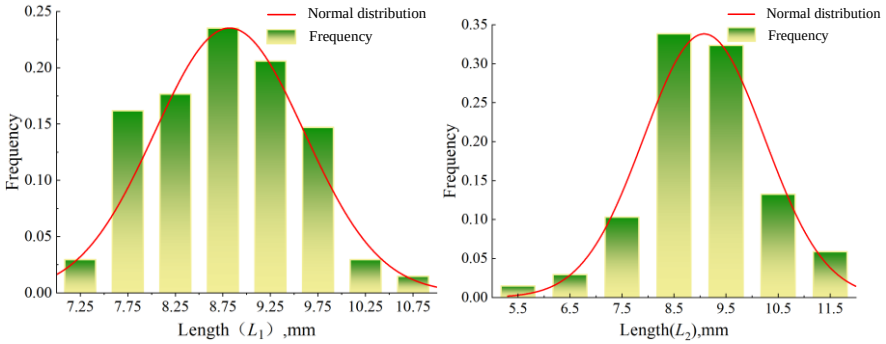

(c) spherical shape

Fig. 5 - Corn seed size and discrete element mode

(a) horse-tooth, (b) prism, (c) spherical

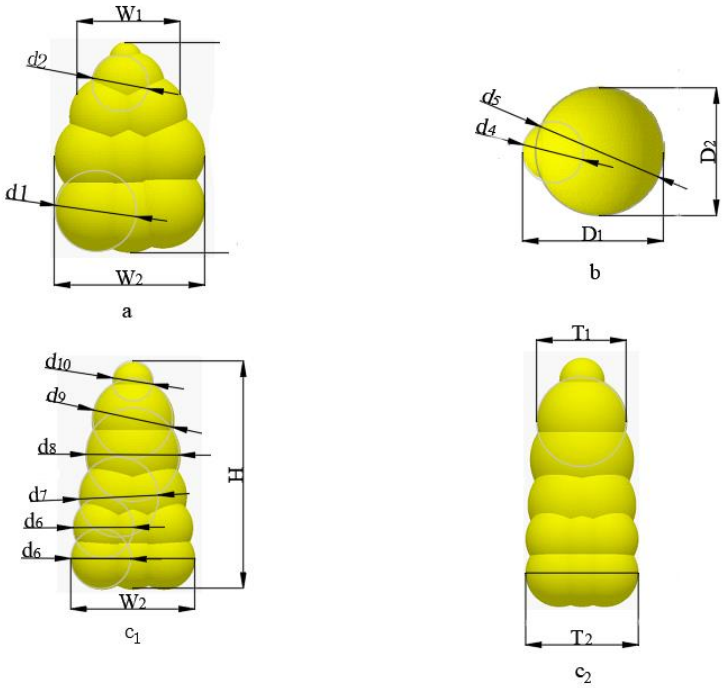

Fig. 6 - A multi-ball filling method for horse-tooth, prism and spherical coated corn seed particle model

(a) Horse-tooth shape; (b) Spherical shape; (c_1) Frontal view of the prism shape; (c_2) The side view of Prism shape.

Formation of the actual angle of repose

The formation process of the plexiglass angle of repose is shown in Fig. 7. 1000 Zhengdan-958 corn seeds are randomly placed into a plexiglass cylinder with an inner diameter of 50 mm. The lower portion of the cylinder tube is attached to the tabletop, and the plexiglass cylinder tube is then lifted vertically and steadily at a rate of 3 mm/s. The angle of repose is the angle between the inclined plane and the horizontal plane of the seed pile. As shown in Fig. 8, the actual seed drop test value is made more precise using computer image processing technology and Matlab software to read the seed drop test image, followed by grayscale and binarization processing to obtain a more precise population accumulation boundary line. Then, in Matlab, invoke cftool to fit the stacked boundary line. As shown in Table 2, the correct value of the angle of repose is the slope of the fitted line; this value is then averaged over the 5 test groups. The angle of repose for the horse tooth is 25.3 °, the angle of repose for the prism is 23.5 °, and the angle of repose for the spherical object is 22.2 °.

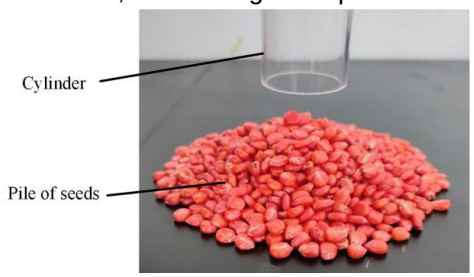

Fig. 7 - Experimental angle of repose of corn seeds

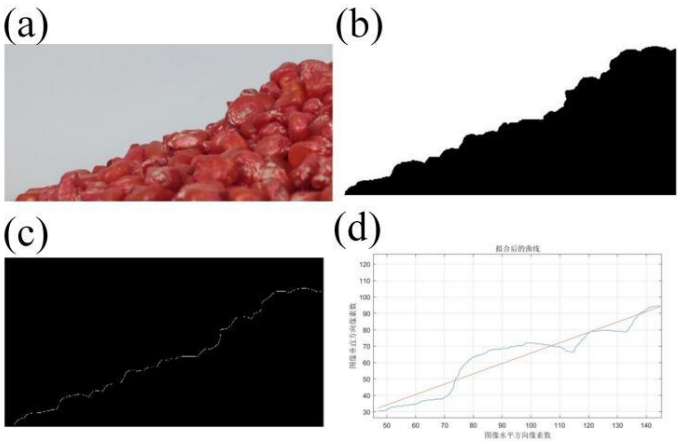

Fig. 8 - The measured value of actual seed dropping test

(a) Original image; (b) Boundary image; (c) Binarized image; (d) Repose angle curve after fitting.

Table 2

Measured repose angles of seed particles with different shapes of coated corn

Material	Angle of repose [°]					Average value [°]	STDEV
Horse-tooth shape	24.7	25.9	26.2	24.7	25.2	25.3	0.62
Prism	24.1	23.7	24.2	22.9	22.7	23.5	0.62
Spherical shape	22.0	22.7	21.9	21.7	22.6	22.2	0.40

Simulation numerical of angle of repose

Angle of repose is a macroscopic quantity that characterizes the flow, friction, and other properties of granular materials. It is related to the physical properties of contact materials and the materials themselves. Before discrete element simulation, it is necessary to identify material characteristic parameters and interaction parameters. Material characteristics include seed size, density, Poisson's ratio, and shear modulus. The form and size of seeds were determined by measuring their triaxial size, and their density was determined by the drainage method to be 1197 kg/m^3. The interaction parameters are the restitution coefficient, the static friction coefficient, and the rolling friction coefficient. The reference contains additional parameters that are required (*Liu et al., 2021*). Among these, measuring methods and theories for the coefficient of restitution of corn seeds and the static friction coefficient of irregularly shaped materials are substantially developed.

The coefficient of restitution between corn seeds, which is 0.37 (*Gonzá et al., 2012*) is one of the important corn seed characteristics required for numerical modeling. Corn seeds of static friction coefficient is 0.2, (*Wang et al., 2017*). Due to the irregular shape of corn, it is difficult to measure the rolling friction coefficient,

and the rolling friction coefficient is the basis of the improved interaction between particles, requiring calibration prior to simulation. Therefore, the study is centered on the rolling friction coefficient across different types of maize species. Table 3 provides a comprehensive list of other attribute settings and interaction parameters.

Table 3

Other parameters required for DEM simulation

Simulation condition	Parameters	Value
Corn seeds	Poisson ratio	0.4
	Shear modulus [Pa]	1.37×108
	Density [kg·m^{-3}]	1197
Organic glass	Poisson ratio	0.4
	Shear modulus [Pa]	2.5×1010
	Density [kg·m^{-3}]	2700
Corn seeds and organic glass	Coefficient of restitution	0.709
	Coefficient of static friction	0.459
	Coefficient of dynamic friction	0.0931

The simulation angle of repose is depicted in Fig. 9, 1000 corn seeds are produced in a tube with a diameter of 50 mm, a radius of 25 mm, a distance of 300 mm between the seed factory and the bottom plate, and a generation rate of 500 seeds per second. Within 2 s, corn seeds are produced, and within 2.1 s, the cylinder begins to rise at a rate of 0.3 mm/s. Due to the lack of restraint provided by the tube wall, the corn at the bottom of the cylinder began to disperse upon lifting the cylinder. After the corn particles had stabilized, the angle of repose was determined.

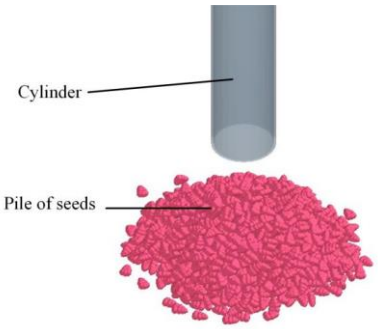

Fig. 9 - Simulation angle of repose test

RESULTS AND DISCUSSION

Interspecific rolling friction coefficient of each corn seed

In order to acquire the interspecific rolling friction coefficient of coated corn seed particles of various shapes, the simulation angles of restate of horse tooth, prism, and spherical corn seed models were determined by varying the rolling friction coefficient in a DEM simulation test. Horse tooth and prism rolling friction coefficients were chosen at 0.001, 0.003, 0.005, and 0.007. The friction coefficients for spherical rolling are set to 0.01, 0.03, 0.05, and 0.07, respectively. Under various rolling friction coefficients, the angles of repose for horse-toothed, prism, and spherical coated corn seed models were measured. By comparing the DEM simulation angle of repose to the actual test angle of repose, more accurate predictions of the interspecific friction coefficients of horse toothed, prism, and spherical corn seeds were made, as depicted in Fig. 10. The projected interspecific rolling friction coefficient for horse-toothed corn seeds was 0.0042, for prism corn seeds it was 0.0032, and for spheroidal corn seeds it was 0.047.

Interspecific rolling friction coefficient of mixed corn seed particles

In order to obtain the interspecific rolling friction coefficient between different corn seed particles, the rolling friction coefficient model of horse tooth and prism corn, horse tooth and spherical corn, prism and spherical corn were mixed with 500 samples each in a DEM simulation test. The rolling friction coefficients of horse tooth shape and prism shape, horse tooth shape, and spherical shape were set to 0.001, 0.005, 0.009, and 0.013, respectively, while the rolling friction coefficients of prism and quasi-circle were set to 0.005, 0.010, 0.015, and 0.02. By comparing the simulation angle of repose obtained by setting different rolling friction coefficients with the simulation angle of repose obtained by the actual experiment, more accurate inter-specific rolling friction coefficients between different shapes of coated corn seed particles were deduced. As shown in Fig. 10, it was predicted that the rolling friction coefficient of horse-toothed and prism corn was 0.0097, that of horse-toothed and spherical corn was 0.0086, and that of prism and spherical corn was 0.0135.

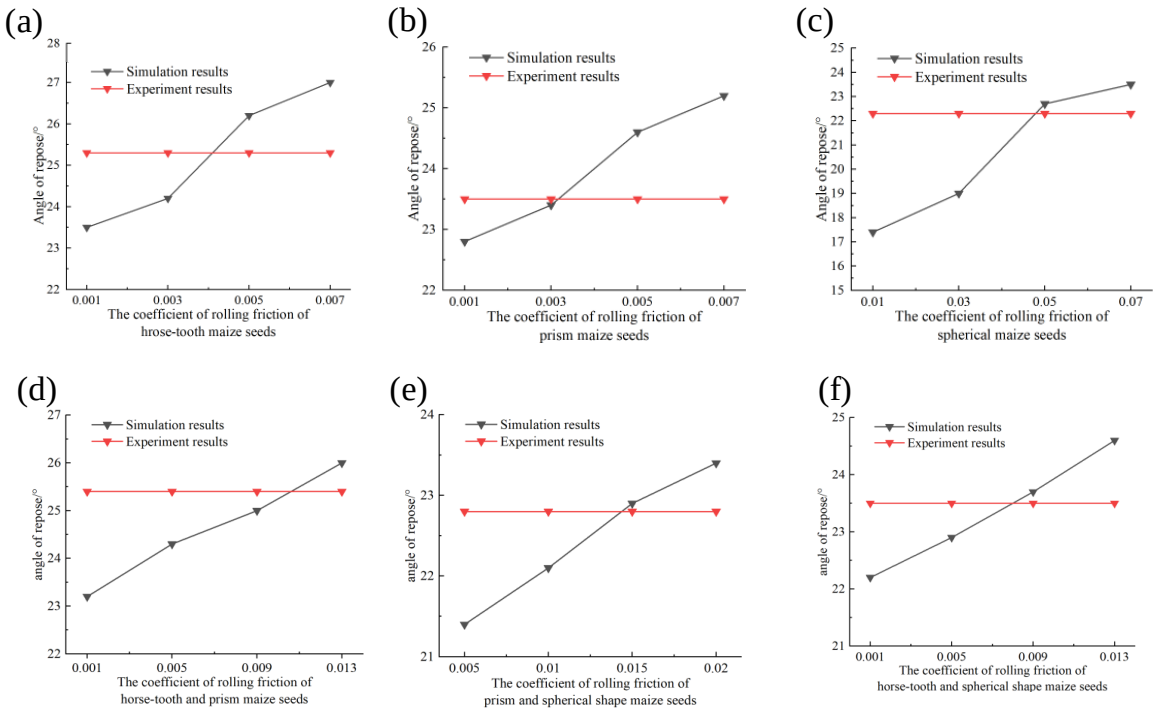

Fig. 10 - Relationship between the coefficient of rolling friction and the repose angle

(a) Horse-tooth shape; (b) Prism shape; (c) Spherical shape.

The effect of seed particle form and rolling friction coefficient on the flow behavior of particles

To investigate the effect of the population flow behavior of corn particles with different shapes on the accumulation process, three distinct types of corn seed particles (horse-tooth shape, prism shape, and spherical shape) were generated above the cylinder and subsequently deposited within it. After filling the cylinder with seed particles, the cylinder began to ascend. As the cylinder was raised upward, the lower seeds lost support from the cylinder wall and began to slip out of the cylinder. During sliding and rolling, particles came into contact with the packing.

The results were shown in Fig. 11 (a), (b), (c) of the horse tooth, respectively, prism and spherical corn under different rolling friction coefficients. At a time of 3.2 s population average velocity diagram, a cylinder at the bottom of the corn, due to the lack of constraints, began to spread around the wall, above and below the corn due to a lack of corn support. Under the influence of gravity, the corn began to descend, and as a result, its gravitational potential energy transformed into kinetic energy and rolled downward. The overall corn height continued to drop, while the spread area continued to grow. The cylinder at the bottom of the corn accumulation had formed a stable state, while at the top, the corn seed particles had greater speed. The horse-tooth shaped maize seed particles were flat, which hindered the movement of the lower group of particles. The corn seed particles on top of the downward movement along the circular pile formed by the corn below the downward slope remain stable. The maize seed particles, which had a high level of sphericity, had good fluidity, resulting in slower speed attenuation compared to particles with a horse tooth shape or pyramid shape. While the upper seeds exhibited a continuous downward flow, the lower group of particles remained unstable and exhibited a specific velocity. As a result, the majority of the corn seed particles located on the upper surface were going to exert pressure on the corn seed particles located beneath them, causing them to disperse. A small portion of it rolls along the circular slope formed below. In the process of forming the angle of repose, the shape of the corn seed particles played a significant role in determining the fluidity of the corn seed particles. Irregular seed particles (horse-tooth-shaped and prism) limited the flow of particle groups, and the more irregular the seed particles in the accumulation process, the more likely it was that a stable state would be formed, which was advantageous to the angle of repose.

As the simulation progressed, the influence of the rolling friction coefficient on the number of falling particles increased; the greater the rolling friction, the lower the population mobility and accumulation rate; conversely, the greater the rolling friction of corn seed particles, the faster the accumulation of particles when there were more seeds in the cylinder and longer distances between the seeds and the cylinder. The longer it took for the seed particles to fall through the stuffing hole and onto the corn bed, the larger the stuffing hole must have been. Spheroidal corn seed particles were the most susceptible to changes in rolling friction coefficient.

Fig. 12 depicted the top view of the seed pile at the time of Fig. 11, where (a), (b), and (c) correspondingly revealed that the horse teeth type seeds had the best fluidity, and the seed diffusion range was the largest in the top view. During the accumulation phase, the flat shape of the horse tooth-shaped corn seed restricted the movement of the corn seed group, resulting in the smallest diffusion area for the horse tooth-shaped corn seed. From largest to smallest, the diffusing areas of diverse corn seed types were spherical, prism, and horse-tooth shaped. The degree of dispersion of corn grains was significantly affected by the varying forms of corn seeds. The angle of repose increased as the rolling friction coefficient increased. This effect occurred because when the corn particles interacted with the contact surface, the coefficient of rolling friction increased, resulting in an increase in rolling resistance. On a flat surface, corn grains did not disperse easily. Consequently, the accumulation area was diminished. Additionally, the greater friction between corn grains made it less likely that the grains would slide down the hill and more likely that they would accumulate.

Influence of particle shape on energy change in accumulation process

The angle of repose test was actually a process of energy conversion. In this process, the potential energy of the kernels would be turned into kinetic energy, and the seeds with kinetic energy would disperse and come to rest gradually, resulting in a larger area of accumulation. Fig.11 depicts the change in potential energy over time for three types of seed particle shapes: horse tooth, prism, and spherical.

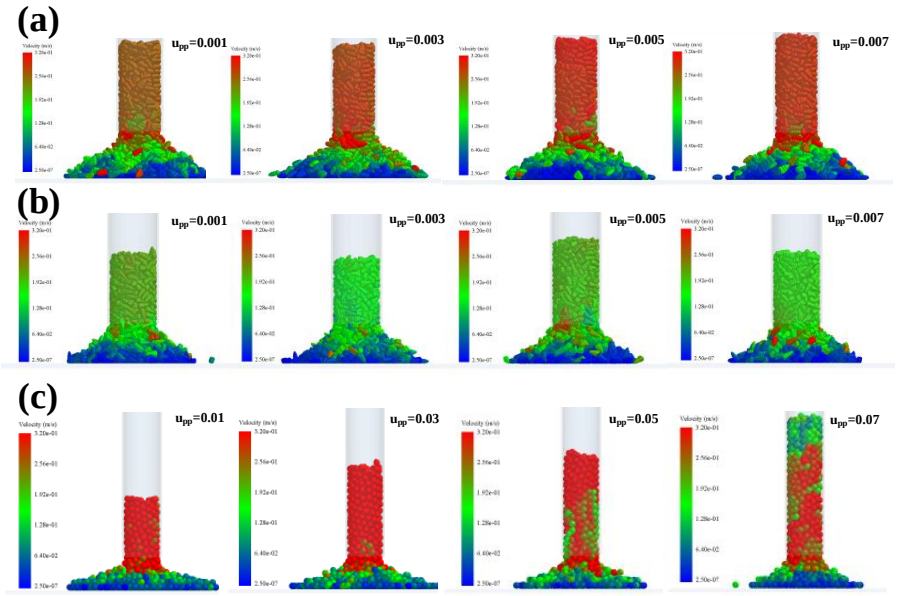

Fig. 11 - Front view of the motion velocity

(a) horse tooth shaped; (b) prism and (c) spherical seed particles under different rolling friction coefficients.

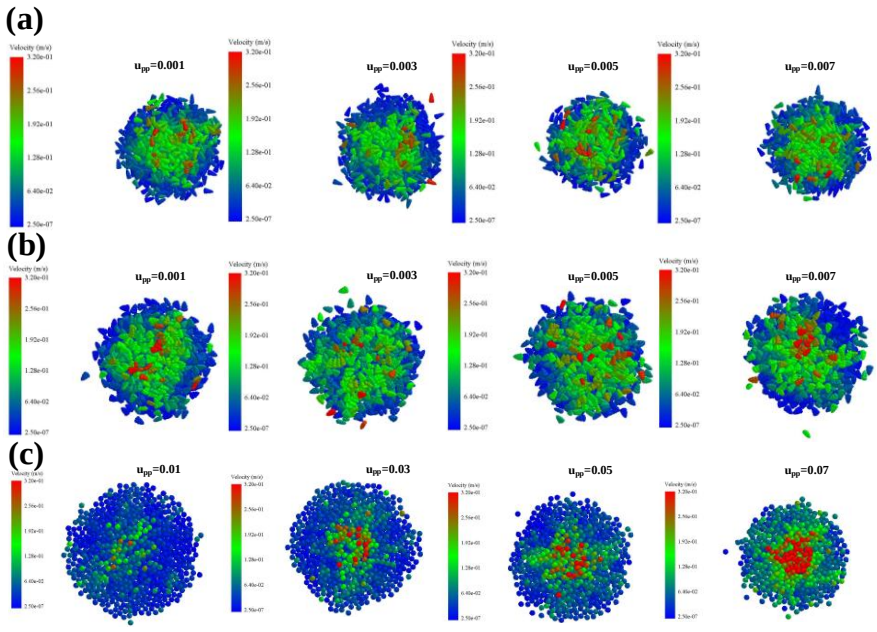

Fig. 12 - Attached view of the motion velocity

(a) horse tooth shaped; (b) prism and (c) spherical seed particles under different rolling friction coefficients.

During the simulation period from 0 s to 1.5 s, as depicted in Fig. 13, three morphologies of corn kernels gradually form while the total potential energy of corn seed particles increases linearly. At 1.5 s, 1000 corn seeds were loaded into the barrel, and between 1.5 s and 2.2 s, the potential energy of seed particles reached an inflection point. Due to the upward movement of the cylinder, the corn seeds in the cylinder would be lifted by the friction of the cylinder wall. At this time, the cylinder lifting height was low. The lower seeds were subject to interspecific friction. The seeds of corn seed particles did not collapse; potential energy had a small improvement in seeds until around 2.5 s, when the constraints completely out of the wall below the seed caused the seed to begin to collapse. Without the support of the seeds below, the top population started to diminish, and the corn fragments kept falling out of the stuffing mouth.

As the corn grain outflows, the total potential energy decreases gradually, especially with the horse tooth shape and type of spherical kernels falling rapidly, reducing the potential energy of the seed. The rolling friction coefficient of corn seed particles with different shapes was different. The descending rate of potential energy was not the same, and the descending rate of potential energy of the spherical seed was the fastest, the potential energy decline rate of the prism seed was much slower than that of the other two shapes of corn seeds. The horse tooth shape had a potential energy of approximately 3.5 s, the prism shape had a potential energy of approximately 3 s, and the spherical shape had a potential energy of approximately 3.2 s, indicating that all the corn seed particles had left the packing and accumulated in the corn pile. The sliding and rolling of corn particles on the corn pile progressively cease due to friction, and the potential energy approaches its stable value.

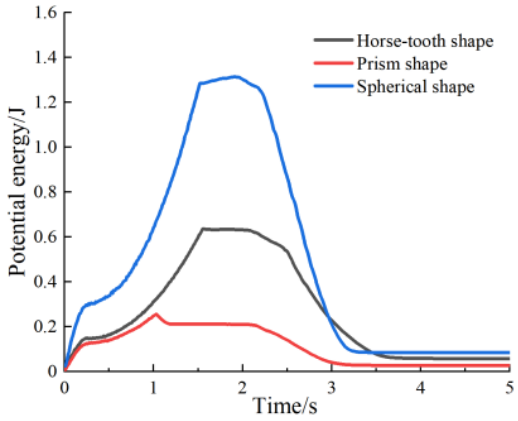

Fig. 13 - Potential energy variation of corn seeds with three shapes during accumulation

Fig.14 depicts the evolution of the average population velocity of three different-shaped corn seeds during the accumulation process. Fig.12 demonstrated that the average velocity of different-shaped corn seed particles first increased, then declined, and finally became static. The average speed of the population swung within 1.5 s-2 s, however, the variation amplitude was minor, as depicted in the graph. After 2 s, the population speed of the three types of corn seeds continued to increase, with spherical, horse-tooth, and prism having the highest average population speed, respectively. The results are shown in Fig.14. The average velocity attenuation rate of corn seed particles with different shapes was distinct, with spherical seed particles having the highest attenuation rate and horse teeth seed particles having the lowest. It was evident that the form of corn kernels was a significant element in preventing their flow.

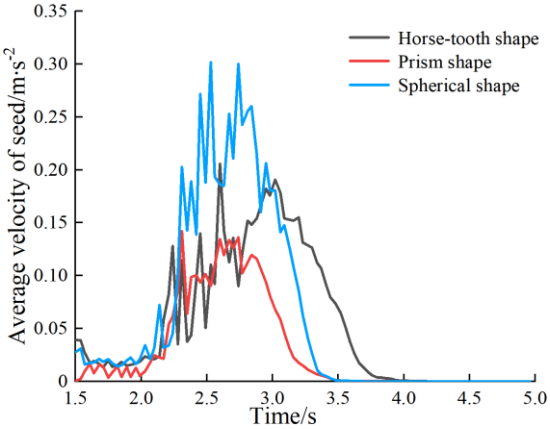

Fig.14 - Plot of average velocity variation of corn seeds of three shapes during accumulation

Influence of seed particle mixing with different shapes on accumulation process

To examine the role of three typical shapes of coated corn seeds in the creation of the angle of repose, the distribution positions of various shapes of corn kernels in the angle of repose are examined. The horse tooth, prism, and spherical corn seeds were mixed with 1000 seeds in a ratio of 43:12:10. In order to make the accumulation process more realistic, three kinds of corn seed particles must be mixed inside the cylinder so that each shape of corn seed particle has good dispersal. Fig.15 depicts the angle of process for three kinds of shapes of corn seed particles.

Starting from 0 s, seed particles of three shapes continued to form and gradually fall and fill the cylinder. At 2 s, the seed particles finished filling the cylinder and began to rise. During the lifting of the cylinder, the seeds began to disperse without the confinement of the cylinder wall. At 5.0 s, the seeds ceased to disperse and accumulated into a seed pile. For better research on the formation of the angle of repose, which played a different role in different shapes of corn seeds, respectively from the seeds of intermediated middle distance and distance of 30 mm thickness for 5 mm slices, as shown in Fig. 16 for the seeds of the slicing process, by examining three different locations of slice, because the horse tooth shape of corn seed particles was more prevalent, the angle of repose played a different role in the formation of these seeds. Therefore, the majority of the section surface was formed of horse tooth-shaped corn seeds, with a few round and prism-shaped corn seeds filling in the gaps. It could be shown that horse tooth-shaped corn grains played a significant role in the height direction of the angle of repose, but prism and spherical corn seed particles played just a little role. Observing the front view and top view of the seed heap between 4.4-5 s in the stacking process of Fig. 15 revealed that the diffusion amplitude of the horse-tooth seed, which occupies a large proportion, was smaller than that of the spherical seed particles in the circumferential direction of the seed heap during the final stacking process. The circumferential direction of the seed pile could be attributed primarily to the spherical corn seeds. Horse tooth and prism corn seed particles performed a supporting role, showing that the sphericity of horse tooth and prism seed was lower and the population mobility effect was bad, whereas the sphericity of quasi-spherical seed was higher and the population mobility effect was better.

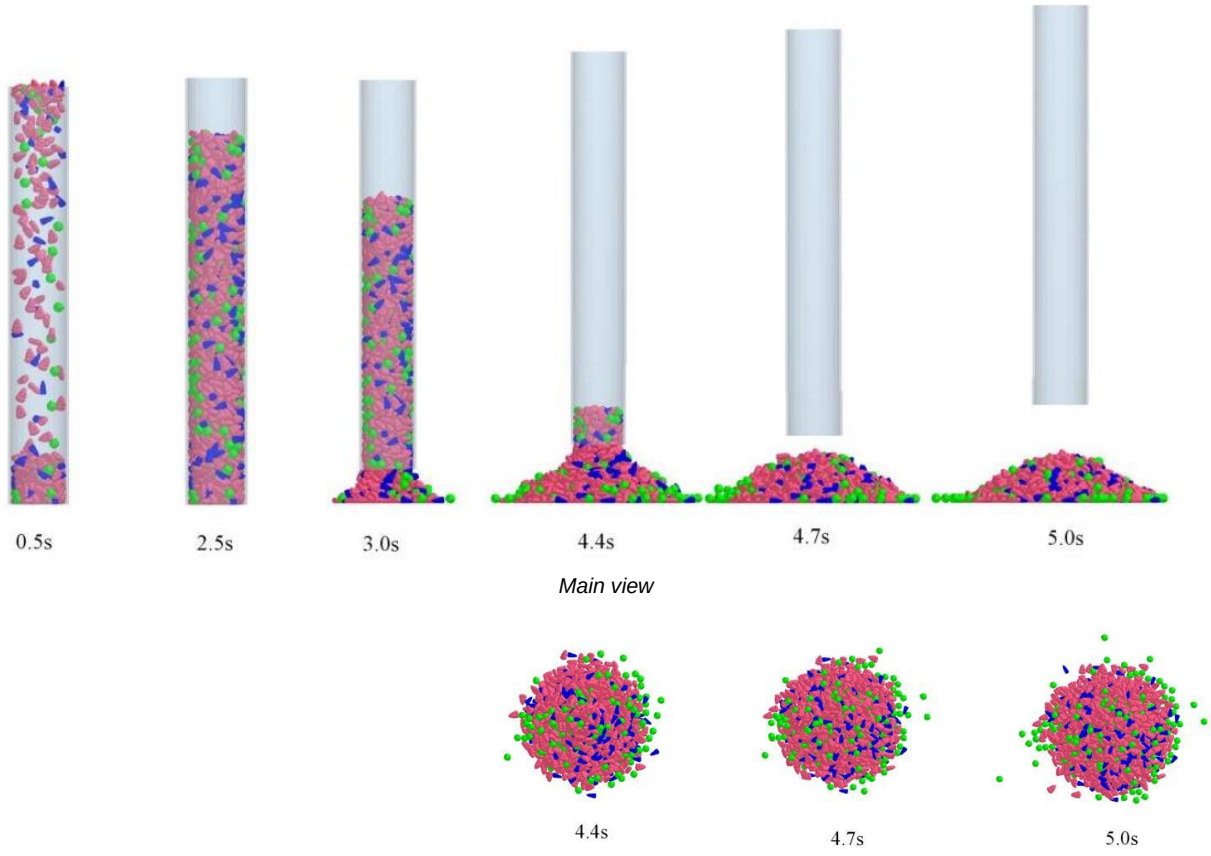

Main view

Top view

Note: Red is horse tooth shape; blue is prism shape; green is spherical

Fig. 15 - Mixed accumulation process of corn grains with different shapes

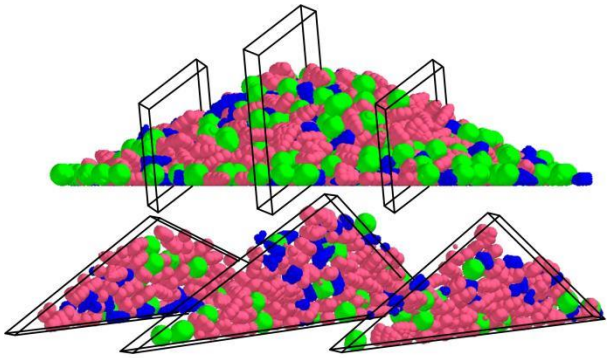

Fig. 16 - Model of slice

Verification test

In this study, the rolling friction coefficient between different corn seed particles was estimated using a combination of practical and simulated testing to validate the rolling friction coefficient approach. 1000 seeds were combined in a proportion of 43:12:10 for horse tooth shape, pyramid shape, and quasi-circle shape under the same conditions. The coefficient for predicting the rolling friction of horse tooth-shaped corn seed was fixed at 0.0042. The prediction coefficient for rolling friction was 0.0032 for the pyramidal corn model and 0.047 for the spherical corn model. The coefficient of rolling friction prediction for horse tooth and pyramid corn seeds was 0.0092, for horse tooth and round corn seeds it was 0.0086, and for pyramid and round corn seeds it was 0.014. After the model was stabilized, 1000 seeds were dropped from above the seed box of the pneumatic corn seed feeder into the seed feeder. The real measurement and simulation tests were done three times, respectively, to observe the seed distribution (Figure 17). The essential feature sizes of the distributions of two major populations were chosen for comparison, as depicted in Figure 17c, and the measured values were presented in Table 3.

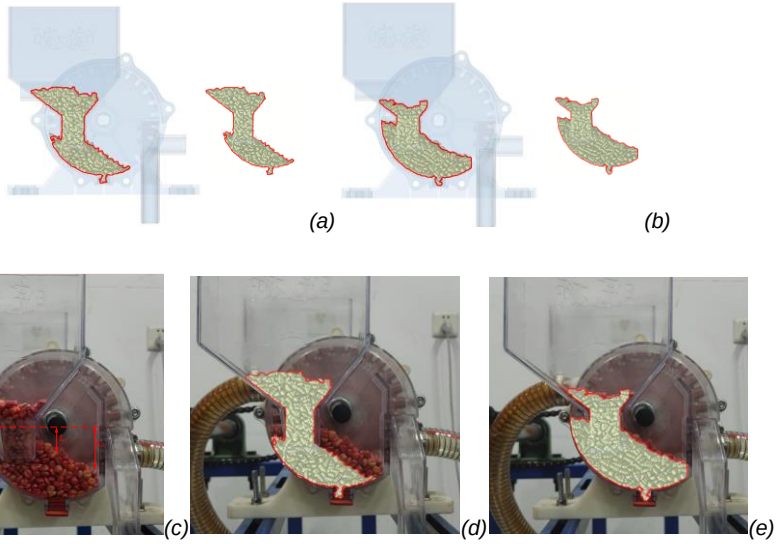

Fig.17 - Comparison of simulation and actual tests

(a) Before calibration; (b) After calibration; (c) Actual measurement; (d) Compare with the actual measurement before calibration; (e) Compare with the actual measurement after calibration.

The measured data indicated that the key size of the population determined by the simulated test with calibrated contact parameters and the measured value differ by less than 5.6%. The calibrated contacted parameters increase the fluidity of the corn coupling model and restore its physical properties to those of actual corn particles. This would ensure the authenticity of the coupling simulation that follows.

Table 4

Comparison of key feature sizes for simulation and actual results

Key feature sizes	Simulation value [mm]	Actual measurement value [mm]	Difference value [%]
L_1	29.47	31.12	5.60
L_2	47.76	50.02	4.73

CONCLUSIONS

In the study, comparative observation was used to pick three typical corn models (including horse teeth shape, prism shape, and spherical shape) with a large proportion of irregularly shaped corn. Three more accurate corn particle models were developed after measuring the real characteristic size of each corn shape and obtaining its positive distribution. The angle of repose of the plexiglass cylinder container was simulated using the rolling friction coefficient of the particle model as the independent variable and the desired value of the simulated angle of repose. The rolling friction prediction coefficients for horse tooth, prism shape, and spherical corn seeds were 0.0042, 0.0032, and 0.047, respectively. The rolling friction prediction coefficients between horse teeth and prism, horse tooth and spherical, and prism and spherical seed were 0.0092, 0.0086, and 0.014, respectively.

To examine the effects of seed particle shape and rolling friction coefficient on seed flow behavior, the motion velocities of three types of corn under different rolling friction coefficients and the potential energy and average velocity of seed particles with different shapes under the same rolling friction coefficient were extracted. In stacking tests with different rolling friction coefficients, the three shapes of corn showed that as the rolling friction coefficient went up, the stacking rate went down, the seed flow got worse, and the time it took for the seeds to leave the cylinder went up. The sensitivity of the spherical form to changes in the rolling friction coefficient was significantly greater than that of the horse teeth and prism shapes.

The three corn models had very different shapes. When the rolling friction coefficient was the same, the spheroidal seed particles with higher sphericity moved more easily than the horse tooth shape and the prism shape of the non-spherical model. Also, the spherical seed particles with better fluidity had a smaller resting angle than the horse tooth shape and the prism shape.

ACKNOWLEDGEMENT

This work was supported by the National Natural Science Foundation of China, China (Grant numbers 52275229), Natural Science Foundation Project of Anhui Province (Grant numbers 1908085MC91).

REFERENCES

[1] Balevičius R., Sielamowicz I., Mróz Z., Kačianauskas R. (2012). Effect of rolling friction on wall pressure, discharge velocity and outflow of granular material from a flat-bottomed bin. *Particuology*, 10(6), 672–682.

[2] Boac J., Casada M., Maghirang R., Harner J. (2010). Material and interaction properties of selected grains and oilseeds for modeling discrete particles. *ASABE*, 53(4): 1201–1216.

[3] Chen H., Zhao S., Zhou X. (2020). DEM investigation of angle of repose for super-ellipsoidal particles. *Particuology*, 50, 53–66.

[4] Chen Z., Yu J., Xue D., Wang Y., Zhang Q., Ren L. (2018). An approach to and validation of corn-seed-assembly modelling based on the discrete element method. *Powder Technology*, 328, 167-183.

[5] Ding L., Yang L., Zhang D., Cui T. (2019). Parametric Design and Test of Seed Cleaning Mechanism of Air-suction Corn Seed-metering Device (气吸式玉米排种器清种机构参数化设计与实验). *Transaction of the Chinese Society Agricultural Machinery*, 50(09):47-56. (in Chinese)

[6] Goniva C., Kloss C., Deen N., Kuipers J., Pirker, S. (2012). Influence of rolling friction on single spout fluidized bed simulation. *Particuology*, 10(5), 582–591.

[7] Gonzá M., Fuentes J., Ayuga-Té L., Ayuga F., (2012). Determination of the mechanical properties of corn grains and olives required for use in DEM simulations. *Journal of Food Engineering*,111(4): 553–562.

[8] Li M., Mitsuoka M., Inoue E., Ye J., Liu J., Yang S., Zeng B., Song X., Okayasu T., Hirai Y. (2020). Design and performance analysis of a seed metering device for a buckwheat seeder adopting discrete element analysis. *J. Fac. Agric. Kyushu Univ*, 65(1), 123–129.

[9] Liu R., Li Y., Liu Z., Liu L., Lv H., (2021). Analysis and Calibration of Discrete Element Parameters of Coated Corn Seed（包衣玉米种子离散元参数分析与标定）.*Transactions of the Chinese Society for Agricultural Machinery*, 52(S0), 1-8. (in Chinese)

[10] Ma W., You Y., Wang D., Yin S., Huan X., (2020). Parameter Calibration of Alfalfa Seed Discrete Element Model Based on RSM and NSGA-Ⅱ（基于 RSM 和 NSGA-Ⅱ的苜蓿种子离散元模型参数标定）. *Transactions of the Chinese Society of Agricultural Engineering (Transactions of the CSAE)*, 51(08): 136-144. (in Chinese)

[11] Owen P., Cleary P., (2012). Prediction of screw conveyor performance using the discrete element method (DEM). *Powder Technology*, 193(3): 269–282
[12] Pasha M., Hare C., Ghadiri M., Gunadi A., Piccione M., (2016). Effect of particle shape on flow in discrete element method simulation of a rotary batch seed coater. *Powder Technology*, 296, 29–36.
[13] Peng F., Wang H., Fang F., Liu Y., (2018). Calibration of discrete element model parameters for pellet feed based on injected section method（基于注入截面法的颗粒饲料离散元模型参数标定）. *Transactions of the CSAM*,49(4), 140–147. (in Chinese)
[14] Shi S., Zhang D., Yang L., Cui T., Zhang R., Yin X., (2014) Design and experiment of pneumatic corn precision seed-metering device with combined holes [J]. *Transactions of the Chinese Society of Agricultural Engineering (Transactions of the CSAE)*, 30(5): 10-18.
[15] Tanaka H., Momozo M., Oida A., Yamazaki M. (2000). Simulation of soil deformation and resistance at bar penetration by distinct element method. *Journal of Terramechanics*, 37(1), 41–56.
[16] Urtė R., Álvaro R., Rimantas K. (2016). Determining the shape of agricultural materials using spherical harmonics. *Comput Electron Agric*, 128, 160–171.
[17] Wang J., Tang H., Wang J., Li X., Huang H., (2017). Optimization design and experiment on ripple surface type pickup finger of precision corn seed metering device. *Int. J. Agric. & Biol. Eng*, 10, 61–71.
[18] Wang L., Li R., Wu B., Wu, Z., Ding Z., (2017). Determination of the coefficient of rolling friction of an irregularly shaped corn particle group using physical experiment and simulations. *Particuology*, 38(6): 185–195.
[19] Wang L., Li R., Wu B., Wu Z., Ding Z., (2018). Determination of the coefficient of rolling friction of an irregularly shaped corn particle group using physical experiment and simulations. *Particuology*, 38, 185-195.
[20] Wang S., Yu Z., Aorigele, Zhang W., (2022). Study on the modeling method of sunflower seed particles based on the discrete element method. *Computers and Electronics in Agriculture*, 198, 107012, ISSN 0168-1699.
[21] Wang X., Yu J., Lv F., Wang Y., Fu H., (2017). A multi-sphere-based modelling method for corn grain assemblies. *Powder Technol*, 28, 584–595.
[22] Wang Y., Lv F., Xu T., Yu J., (2018). Soybean seed shape and size analysis and its modelling (大豆籽粒形状和尺寸分析及其建模). *J. Jilin University. Engineering and Technology Edition*, 48 (02), 507–517.
[23] Wang Y., Wang X., Chen Z., Yu J., (2018). Corn seed modeling based on discrete element method (基于离散元法的玉米籽粒建模). *J. Jilin University. Engineering and Technology Edition*, 48 (05), 1537–1547. (in Chinese)
[24] Wu M., Cong J., Yan Q., Zhu T., Peng X., Wang Y., (2020). Calibration and experiments for discrete element simulation parameters of peanut seed particles（花生种子颗粒离散元仿真参数标定与试验）. *Transactions of the Chinese Society of Agricultural Engineering (Transactions of the CSAE)*,36(23): 30-38. (in Chinese)
[25] Xiao L., Björklund S., Rosén B., (2007). The influence of surface roughness and the contact pressure distribution on friction in rolling/sliding contacts. *Tribology International*, 40(4), 694–698.
[26] Xu J., Wang X., Zhang Z., Wu W., (2020). Discrete element modeling and simulation of soybean seed using multi-spheres and super-ellipsoids. *IEEE Access*, 8, 222672–222683.
[27] Yung K., Xu Y., (2003). Non-linear expressions for rolling friction of a soft ball on a hard plane. *Nonlinear Dynamics*, 33(1), 33–41.
[28] Zhang S., Zhang R., Chen T., Fu J., Yuan H., (2022). Calibration of Simulation Parameters of Mung Bean Seeds Using Discrete Element Method and Verification of Seed-metering Test（绿豆种子离散元仿真参数标定与排种试验）. *Transaction of the Chinese Society Agricultural Machinery*, 53(03): 71-79. (in Chinese)
[29] Zhou L., Yu, J., Wang Y., Yan D., Yu Y., (2020). A study on the modelling method of corn-seed particles based on the discrete element method. *Powder Technology*, 374, 353-376.